Solidification behaviour and the effects of homogenisation on the structure of an Al–Cu–Mg–Ag–Sc alloy

Marat Gazizov[a,*], Viktor Teleshov[b], Valerij Zakharov[b], Rustam Kaibyshev[a]

[a] Laboratory of Mechanical Properties of Nanostructured Materials and Superalloys, Department of Materials Science, Belgorod State University, Belgorod, Pobeda 85, 308015, Russia
[b] All-Russian Institute of Light alloys, Moscow, Gorbunova 2, 121596, Russia

A B S T R A C T

The solidification behaviour and structural evolution during homogenisation annealing of a 0.17 mass% Sc and 0.1 mass% Ge modified Al–Cu–Mg–Ag alloy was examined. The formation of the primary Mg_2Ge phase and the Sc-enriched θ-phase (Al_2Cu) was found to occur under solidification; no evidence for the formation of the ternary W-phase ($Al_{8-x}Cu_{4+x}Sc$) was observed. Approximately 70% of the overall Sc content is fixed in the supersaturated solid solution. However, only two thirds of this Sc is consumed by the formation of a dispersion of nanoscale Al_3Sc particles within the Al matrix under homogenisation annealing. A third of the Sc is consumed by the formation of the W-phase because of Sc diffusion into the primary θ-phase, which leads to its transformation into the W-phase. Finally, the W-phase consumes ~50% of the overall Sc content. No effects of homogenisation annealing on the volume fraction of Mg_2Ge were observed. The optimal chemical composition of alloys in the Al–Cu–Mg–Ag–Sc system is discussed.

Keywords:
High-temperature alloy
Rapid-solidification
Precipitation
Thermal analysis
Scanning electron microscopy
X-ray diffraction

1. Introduction

More than 50 years ago, the demand for creep-resistant aluminium alloys led to the development of several age-hardenable aluminium alloys, such as AA2618, AA2014 and AA2219. However, these alloys are no longer able to meet the new requirements for structural aircraft materials. A new generation of airframes, supercharger impellers and fan blades requires aluminium alloys with higher yield stresses, increased creep resistances and crack-propagation resistances in the temperature interval of 150–180 °C [1]. The most promising approach to improving the mechanical properties of Al–Cu alloys at elevated temperatures is additional alloying with elements such as silver and scandium, which are highly effective in precipitation hardening because of the formation of coherent dispersoids. This alloy design philosophy has been used to develop alloy AA2139, which is a member of the Al–Cu–Mg–Ag alloys [1–10] and has recently become commercially available.

Most of the age-hardenable aluminium alloys are limited to application temperatures of 100 °C or less because continuous exposure to higher temperatures results in a rapid coarsening of coherent and semi-coherent dispersoids that are responsible for alloy strengthening [2]. The Al–Cu–Mg–Ag alloys exhibit the highest creep resistance among aluminium alloys of the 2XXX series because of the formation of the Ω-phase, which is believed to be a coherent form of the equilibrium θ-phase. Consequently, coherent Ω-phase dispersoid with plate-like shapes exhibit high thermodynamic stability [1–3]. Coherency between the Ω-phase and the aluminium matrix is maintained along the $\{1\,1\,1\}_{Al}$ habit planes because of the equilibrium segregation of magnesium and silver at the dispersoid/matrix interface [2]. These segregations reduce the coherency misfit strain and provide a low energy for these coherent boundaries. As a result, this phase exhibits superior resistance to coarsening; no loss of coherency takes place under creep conditions at $T \leq 250$ °C [2,3,5,8–10]. Excellent fracture toughness and crack-propagation resistance of the AA2139 alloy also result from the coherent nature of the Ω-phase/Al-matrix interfaces [1,2].

Sc forms Al_3Sc dispersoids that exhibit an ordered fcc lattice of the Cu_3Au type with the $L1_2$ structure; the lattice parameter of this β′-phase (4.105 A) is only 1.6% greater than that of the Al matrix (4.04 A) [13–17]. The primary benefits of the addition of Sc to Al–Cu–Mg–Ag alloys are as follows:

(i) extensive grain refinement of aluminium castings under solidification because of the formation of the primary Al_3Sc phase with incoherent boundaries that exhibit a cusped cubic morphology and a size of 1 μm or higher [11–14];
(ii) dispersion hardening because of the formation of Al_3Sc particles with sizes less than ~50 nm [16–20]; these dispersoids are

* Corresponding author. Tel.: +7 4 72 258 5456; fax: +7 4 72 258 5456.
E-mail addresses: gazizov@bsu.edu.ru (M. Gazizov), vadimus2004@gmail.com (V. Teleshov), vadimus2004@gmail.com (V. Zakharov), rustam_kaibyshev@bsu.edu.ru (R. Kaibyshev).

coherent with the matrix and contribute to the alloy strength through dislocation–particle interactions, such as the case in nickel-based superalloys [14–20].

These two claims obviously have opposing characteristics: Sc-containing aluminium alloys may exhibit a refined solidification structure because of coarse, incoherent Al_3Sc particles, or they may exhibit high strength because of coherent nanoscale Al_3Sc dispersoids, but they rarely exhibit both properties. To form nanoscale particles of the β′-phase, most of the scandium atoms must be fixed within a supersaturated solid solution during solidification. Coherent dispersoids of the Al_3Sc phase must precipitate continuously through nucleation and growth from supersaturated solid solutions under homogenisation annealing, i.e., a bulk decomposition process of the supersaturated solid solution of Sc in Al must occur, and it must result in a high-density dispersion of coherent particles. These dispersoids must be uniformly distributed within aluminium matrix. In contrast, an extensive refinement of the grain size of aluminium castings takes place when the Al_3Sc phase forms as the primary phase in the melt on solidification [12,13]; these particles act as heterogeneous nuclei for α-aluminium during solidification. The formation of a significant amount of coarse particles of the primary Al_3Sc-phase consumes a significant amount of Sc. As a result, less Sc is available for the formation of the nanoscale dispersoids, which diminishes the strengthening effect of Sc [20]. In addition, coarse primary particles deteriorate the crack-propagation resistance. This study was aimed at using approach (ii) to enhance the moderate-temperature performance and improve the mechanical properties of an alloy in the Al–Cu–Mg–Ag system.

Little use of Sc has taken place in the 2XXX series of alloys because of the formation of the ternary W-phase, which has been suggested to be of $Al_{8-x}Cu_{4+x}Sc$ compound [14,19,21,22]. The W-phase forms as coarse particles instead of the β′-phase in alloys with a high Cu/Sc ratio, which diminishes the positive effect of Sc on the mechanical properties of the alloy [14]. Understanding the W-phase precipitation reaction (nucleation and growth) is thus crucial to the development of new alloys in the Al–Cu–(Mg–Ag)–Sc system.

Consequently, the primary aim of the present study was to explore the solidification behaviour of an Al–Cu–Mg–Ag–Sc alloy and the important issue of scandium's apparent ability to produce a dispersion of coherent $Al_3(Sc,Zr)$-phase dispersoids. As previously discussed, the development of new heat-resistant Al–Cu alloy by the incorporation of Sc additives is a complicated task because of the necessity to hinder the precipitation of primary Al_3Sc phase or the formation of the ternary W-phase to provide significant dispersion hardening. We presumed that Sc and Ag additions might mutually affect the formation of the Ω-phase and β′-phase, respectively. However, the literature contains no information concerning this effect.

The second aim of the present study was to examine the effects of elements such as Zr and Ge on the formation of the β′-phase and Ω-phase, respectively, with the intention of enhancing the of mechanical properties of the Al–Cu–Mg–Ag–Sc alloys. Coherent dispersoids of the Al_3Sc phase are highly resistant to coarsening at up to a temperature of ~300 °C, which provides enhanced creep resistance of Sc-containing Al alloys [14,16–18]. Zr is soluble in Al_3Sc, and Zr additives highly impede coarsening of the β′-phase at high temperatures and thus improve creep resistance of Sc-containing alloys [14,19,20,23–25]. In addition, coherent $Al_3(Zr,Sc)$ dispersoids remain intact after homogenisation annealing at high temperatures [14]. Furthermore, a small amount of Zr added to Al–Sc alloys decreases the amount of Sc required to produce strong dispersion hardening, which is important because Sc additives are expensive. The misfit δ between the Al matrix and the $Al_3(Zr,Sc)$ is controlled by the Sc/Zr ratio [14]; coherent dispersoids are evolved if Sc/Zr ≥ 1.5. In the present study, a Sc/Zr ratio of 1.5 was chosen to induce the formation of coherent $Al_3(Sc,Zr)$ dispersoids to achieve greater strength [19]. It is worth noting that authors [15] demonstrated that incoherent Al(Sc,Zr) dispersoids enhance strength of the Al–Cu–Mg–Ag–Sc alloys.

The addition of trace quantities of Ge to Al–Cu–Mg alloys has resulted in considerable refinements of the θ′-phase (Al_2Cu) precipitates [26]. We expected to observe a similar effect of Ge on the precipitation process in Al–Cu–Mg–Ag alloys, and this study was conducted to explore this possibility.

To achieve these goals the solidification behaviour of a 0.17% Sc and 0.12% Zr modified Al–5.6% Cu–0.7% Mg–0.6% Ag alloy and the evolution of its structure under homogenisation annealing was examined in detail. A two-step homogenisation annealing was used to precipitate dispersoids of the β′-phase during a low-temperature step. A high-temperature step of homogenisation annealing was applied to provide the complete dissolution of metastable phases and the uniform distribution of alloying elements within the Al matrix. Significant attention will be given to the determination of the amount of Sc is consumed during the formation of the coarse particles with incoherent boundaries.

2. Experimental details

An alloy with a chemical composition of Al–5.6Cu–0.72Mg–0.5Ag–0.17Sc–0.12Zr–0.32Mn–0.07Ti–0.1Ge–0.02Ni–0.03Fe–0.01Si–0.02V (in mass%) was manufactured by semi-continuous casting using a water-cooled copper chilled mold with a 38 mm diameter, which provided a solidification rate of ~70 K/s. A two-step homogenisation annealing was applied that consisted of a low-temperature step at 360 °C for 6 h followed by a high-temperature step at 510 °C for 24 h. To determine the effect of the homogenisation annealing on the structure, sections were taken from different positions along the centre line of both the cast and the homogenised ingots, and samples were prepared for optical and electron microscopy. Details of the sample preparation for metallographic studies and transmission electron microscopy have been described elsewhere [27,28]. Metallographic analysis was performed using an Olympus GX70 optical microscope; the mean linear intercept method was used to measure the average grain size [12]. The thin foils were examined using a JEOL-2100 TEM with a double-tilt stage at an accelerating potential of 200 kV; the instrument was equipped with an INCA energy-dispersive X-ray (EDX) spectroscope. A Quanta 600FEG scanning electron microscope (SEM) was used for high-resolution EDX microanalysis of the constituent phases on at least six arbitrarily selected typical particles for each data point. Chemical composition is stated as both mass% and at.% in the figures; however, only mass% values are used in the text. Particles with typical chemical compositions are presented in the figures.

Differential thermal analysis was performed on specimens with weights ranging from 60 to 80 mg and exhibiting a disc shape. The samples were scanned at a constant heating rate of 10 °C/min using a SDT Q600 TA Instruments differential scanning calorimeter. Phase analysis was carried out by X-ray diffraction (XRD), using a Rigaku Ultima IV diffractometer equipped with a Cu K_α radiation source and a semi-conductor detector. The samples were scanned over the 2θ interval 15–130° with an angular velocity of 2°/min. A rotating sample holder was used to correct for the effects of preferred orientation.

3. Results

3.1. Microstructure

3.1.1. Solidification structure

Fig. 1 shows typical solidification structures in their as-cast condition. The average grain size is ~300 μm, and the dendrite arm spacing (DAS) is ~30 μm (Fig. 1*a*). Careful inspection of this structure and the solidification structures presented elsewhere [11,12,15,27,29] shows that complex alloying by Sc and Zr provides remarkable refinement of the columnar grains that contain the dendritic substructure; DAS was significantly reduced. However, no formation of fine equiaxed grains without a visible dendritic substructure within its interiors was observed, which is typical for Al–Cu alloys that contain more than 0.3% Sc [11,12,15]. Thus, Sc and Zr additives slightly refine the α-Al grains and highly refine the interdendritic eutectic structure. The amounts of these elements are insufficient to inhibit the growth of the dendritic substructure [11]. Non-uniform etching (Fig. 1) is indicative of a significantly

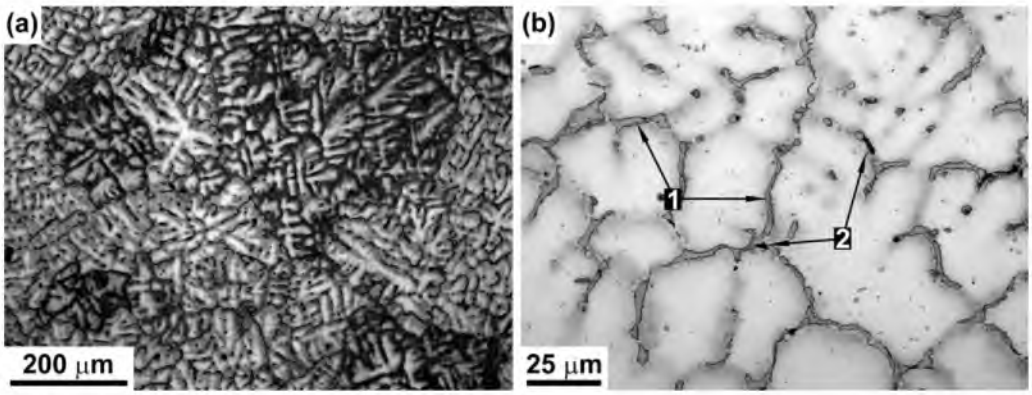

Fig. 1. Examples of solidification microstructures (a) microstructure (b) phases: 1 – bright phase and 2 – dark phase.

non-uniform distribution of alloying elements within the dendrite cells.

Coarse particles of secondary phases are distributed both within the interiors of dendrite cells and on the dendrite boundaries that comprise the shell. Two types of phases could be distinctly distinguished because of well-defined differences in their morphology and colour after phase etching: bright and dark phases. A bright phase exhibits an essentially equiaxed shape within the dendrite

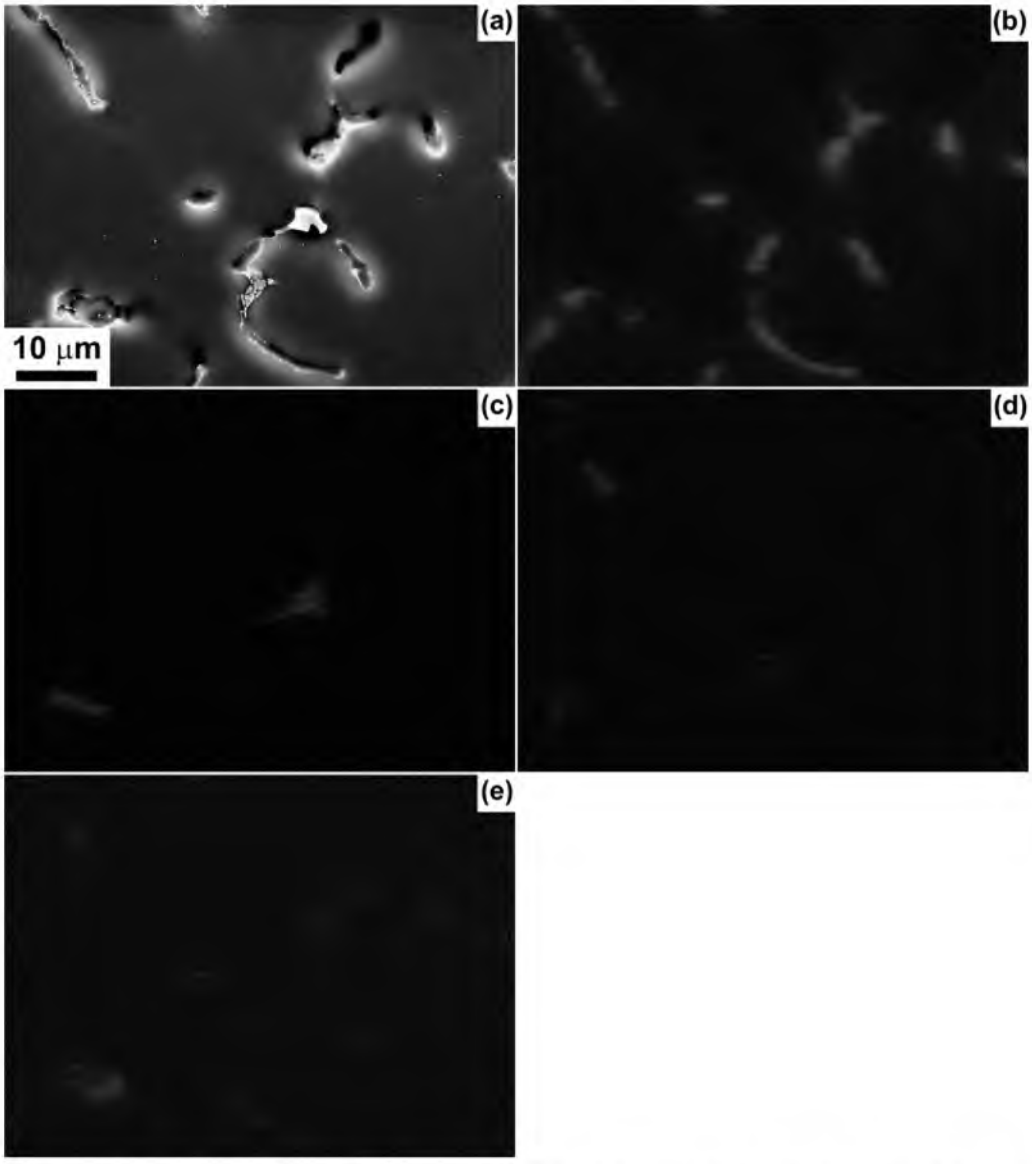

Fig. 2. SEM of solidification structure (a); (b), (c), (d) and (e) are the distribution of element Cu, Ge, Ag and Sc in the selected plane, respectively.

cells. In addition, this phase forms shell-outlining dendrite cells (Fig. 1b). The bright phase is believed to be the θ-phase (Al_2Cu); this phase resembles the θ-phase observed for a "divorced" eutectic [30]. Small particles of the dark phase are usually surrounded by shells of the bright phase. In addition, the dark phase can comprise the shell along the dendrite boundaries together with the bright phase. A minor portion of the dark-phase particles exhibit an equiaxed shape. However, most of the dark-phase particles exhibit irregular shapes. The dark phase could not be interpreted using a metallographic handbook; their morphology is distinctly different from the morphology of the W-phase particles, which are dark after etching [19].

Fig. 2 shows the SEM microstructure and the element mapping of Cu, Ge, Ag and Sc elements. The Cu, Ge and Sc are non-uniformly distributed within the Al matrix. The EDX analysis revealed the presence of three main phases: α-Al, θ-phase (Al_2Cu) and Mg_2Ge (Fig. 3A, C and D, respectively). The morphologies of the C and D phases resemble the morphologies of the bright and dark phases, respectively (Fig. 1b). The Sc tends to segregate within the θ-phase (Figs. 2 and 3); its average content within this phase is 0.6% (Fig. 3C). No evidence for the formation of the primary $Al_3(Sc,Zr)$ phase was observed. The overall Sc content within α-Al is 0.12% (Fig. 3A). The distribution of Sc and Cu within the primary θ-phase is essentially non-uniform (Fig. 8a). Thus, approximately 70% of the Sc was fixed within a supersaturated solid solution during solidification. The cooling rate used in the present study was sufficient to trap almost all of the Zr in solution upon freezing, thus forming no primary particles or segregation within the θ-phase (Fig. 8a).

The particles that exhibit dark-phase morphologies contain a high proportion of Ge (Figs. 2 and 3) and were identified as the Mg_2Ge phase. We assume that these particles also contain Mg, although we cannot prove this directly because the single, well-defined X-ray line of Mg (Kα at 1.252 keV) matches that of Ge (Lα1 at 1.1 keV).

In general, Ag and Mg are uniformly distributed within the Al matrix. However, evidence of Ag- and Mg-containing phases was occasionally found (Fig. 3B). These particles contain a high proportion of copper (Fig. 3B). The specific contrast of such particles is indicative of their complex structure.

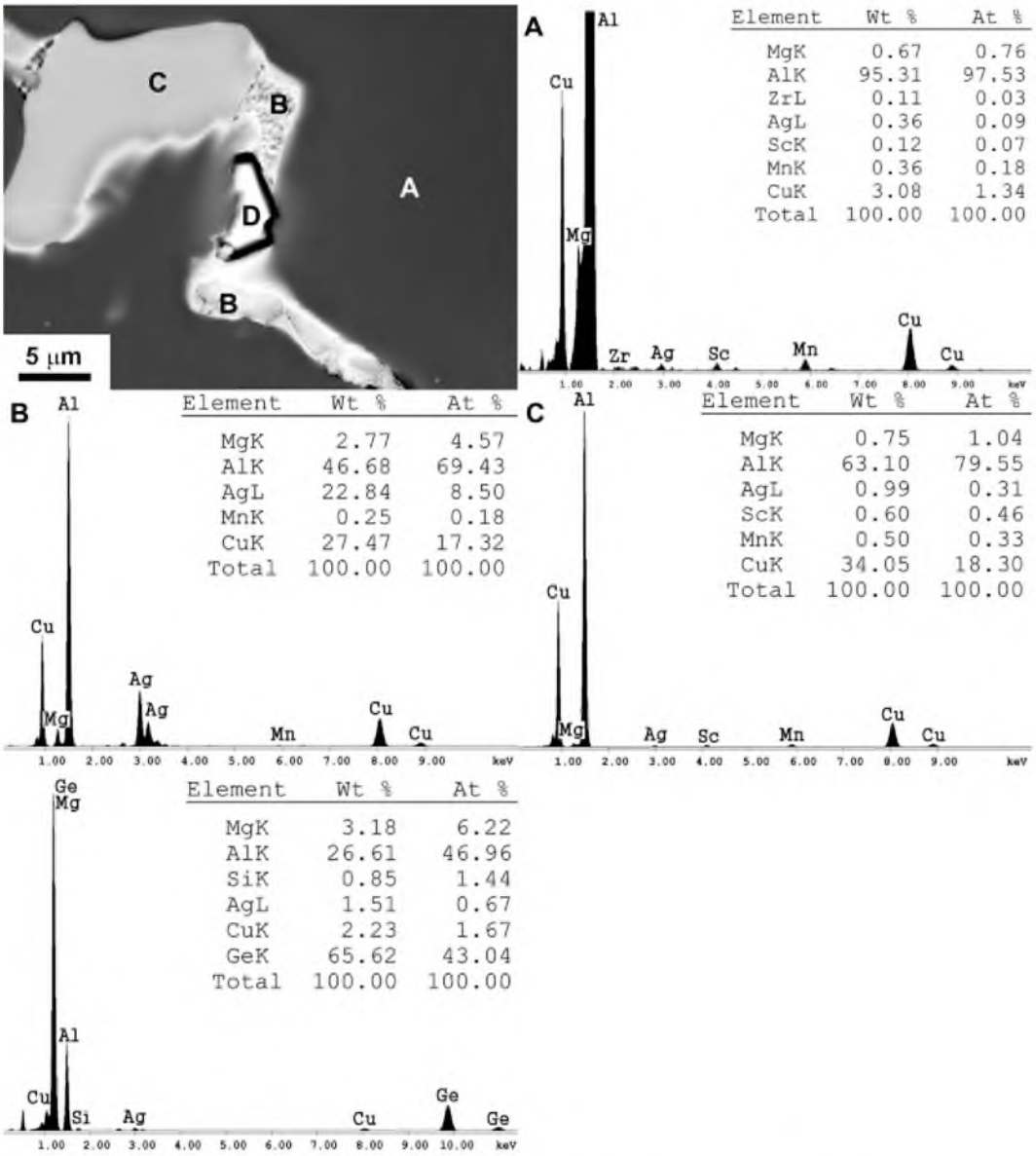

Fig. 3. SEM image of the as-cast alloy (a) and EDX analysis of particles indicated as A, B, C and D.

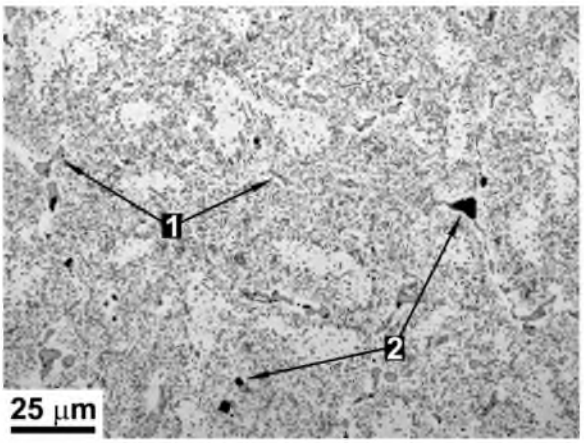

Fig. 4. Typical microstructure after homogenisation annealing: 1 – bright phase and 2 – dark phase.

The formation of the following primary phases takes place under solidification: (i) θ-phase enriched by Sc; (ii) Mg_2Ge phase; and (iii) a phase of unknown origin that contains Ag and Mg. The formation of the primary θ-phase consumes more than 30% of the Sc.

3.1.2. Structure after homogenisation annealing

The microstructures of the samples after the homogenisation annealing are presented in Figs. 4–7 and 8b. The dissolution of the excessive θ-phase occurs both within the dendrite cells and along the dendrite boundaries; the volume fraction of the primary particles of the θ-phase decreases from 4.9 to 1.2%. The present alloy is a hypoeutectic alloy, and several particles of the primary θ-phase, which is the equilibrium phase, remain non-dissolved. The uniform distribution of alloying elements can be detected from metallographic observations (Fig. 4).

The SEM images and the elemental mappings of Al, Cu, Ge, Ag, and Sc (Figs. 5–8) indicate that particles of two different phases that contain copper and scandium can be clearly distinguished (Fig. 5): (i) coarse particles of the W-phase that contain ~5.6% Sc, ~2% Zr and ~50% Cu and (ii) fine particles of the θ-phase that contain 1.6% Sc. The atomic ratio between Al and Cu is 86:10 (Figs.

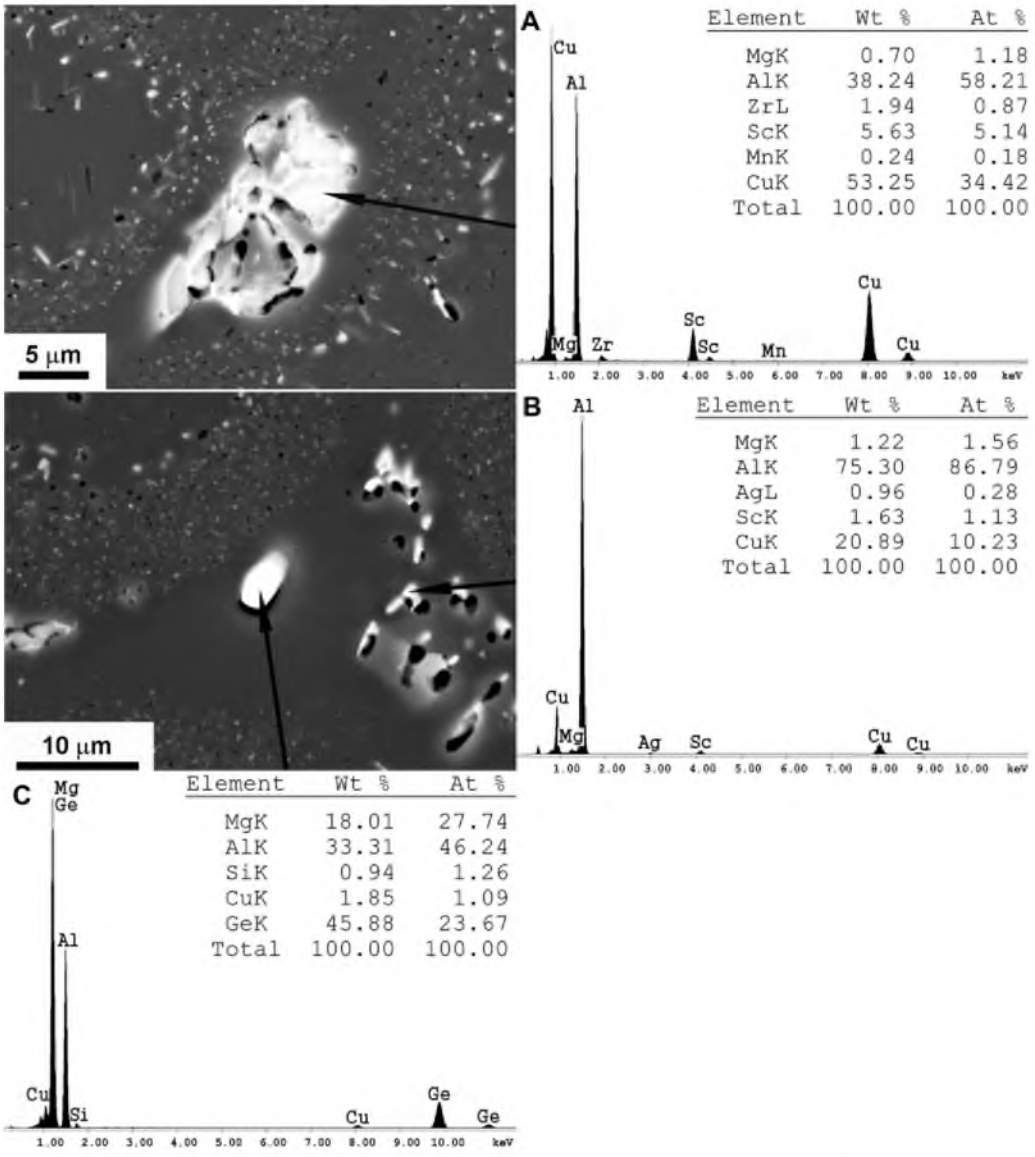

Fig. 5. SEM image after homogenisation annealing (a) and EDX analysis of particles indicated as A, B and C.

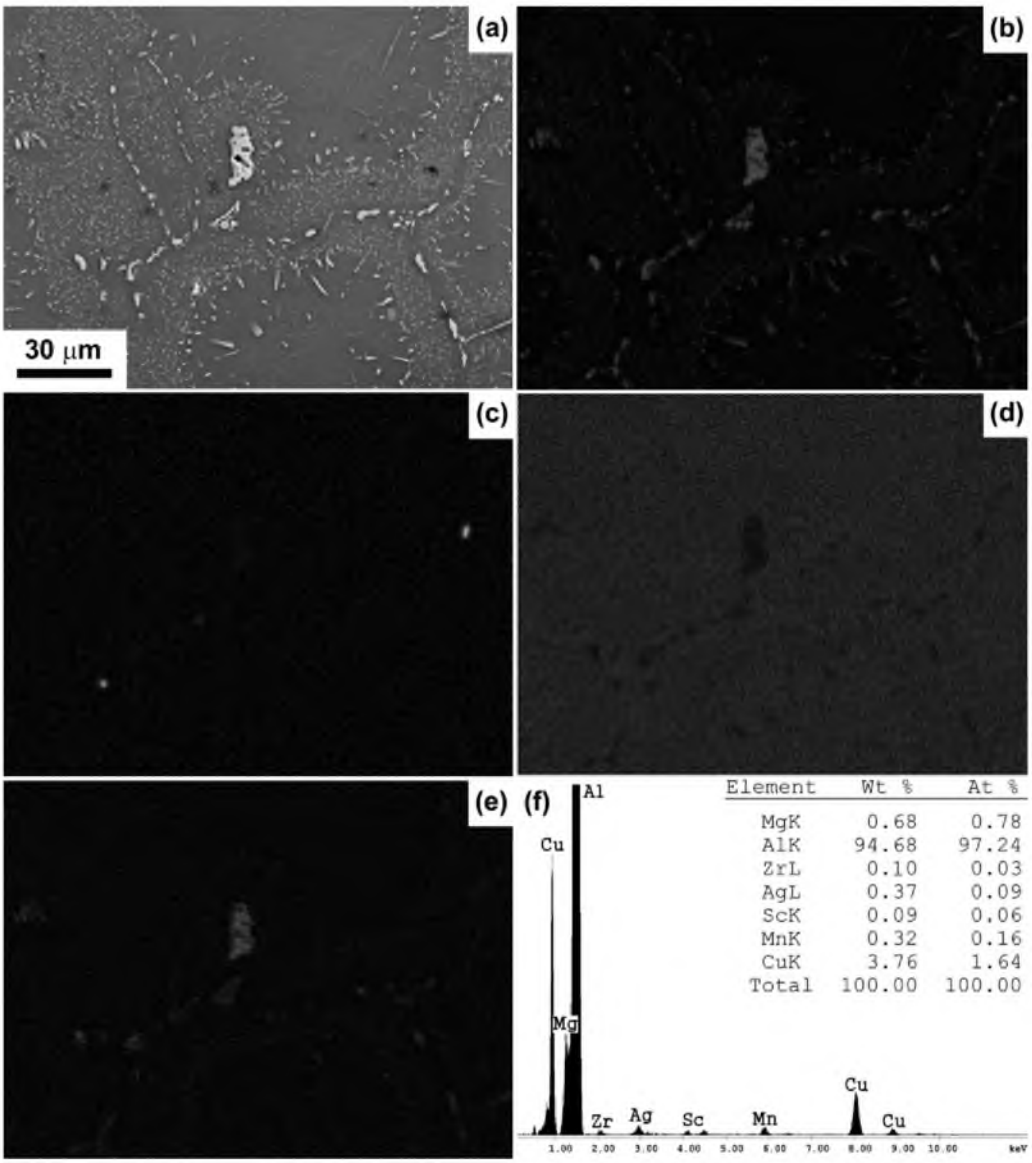

Fig. 6. SEM image after homogenisation annealing (a); (b), (c), (d) and (e) are the distribution of Cu, Ge, Ag and Sc in selected plane, respectively; chemical composition of matrix (f).

5B and 8b), or approximately 8.6:1 within this θ-phase. The distribution of Sc and Cu become essentially uniform within this θ-phase, whereas Zr tends to segregate slowly within this phase (Fig. 8b). The sum of Sc and Zr (Sc+Zr) in the ternary W-phase, on average, is approximately equal to the Sc content (9.3%) in this phase reported elsewhere [19,21]. The W-phase and Sc-enriched θ-phase could be observed as isolated particles (Figs. 5b and 8b), but they were also observed in mutual contact (Fig. 7). The particle depicted in Fig. 7 was found to contain both several separate W-phase areas that were enriched by Sc and Sc-depleted θ-phase regions (according to the composition analysis). Therefore, this particle is referred to as a hybrid particle [31], and most of particles identified as particles of the W-phase in the present study were hybrid particles. The W-phase exhibits an irregular shape wedge within the body of the θ-phase, and the θ-phase/W-phase interface is distinctly distinguished (Fig. 7). These observations are consistent with a straightforward chemical transformation of the θ-phase into the W-phase by the incorporation of Sc from the surroundings. As a result, Sc depletes from the adjacent θ-phase (Fig. 7). In addition, the growth of separate W-phase particles is apparently accompanied by the dissolution of separate fine particles of the Sc-enriched θ-phase (Figs. 5, 6, and 8b): coagulation of Sc-containing particles is accompanied by the transition from the θ-phase to the W-phase.

The analysis of the elemental mapping (Figs. 5 and 6) and metallography (Fig. 4) shows that almost all of the particles of the Mg_2Ge phase assume equiaxed shapes; their volume fraction remains unchanged. Silver is very uniformly distributed within α-Al; no silver segregation within the particles was observed. Coarse particles are almost free from Ag (Fig. 6d). The phase of unknown origin that contains Ag and Mg completely dissolves during homogenisation annealing.

The TEM observations reveal a dispersion of nano-scale particles within the aluminium matrix after the homogenisation annealing (Fig. 9). These dispersoids exhibit the specific "bean-coffee" contrast, which suggests their coherent origin [32]. Their average size is 25 nm, and their distribution is uniform at the micro-scale level within the grains (Fig. 8). These particles were identified as $Al_3(Sc,Zr)$ dispersoids by EDX analysis and by examination of selected diffraction patterns. Their volume fraction is strongly

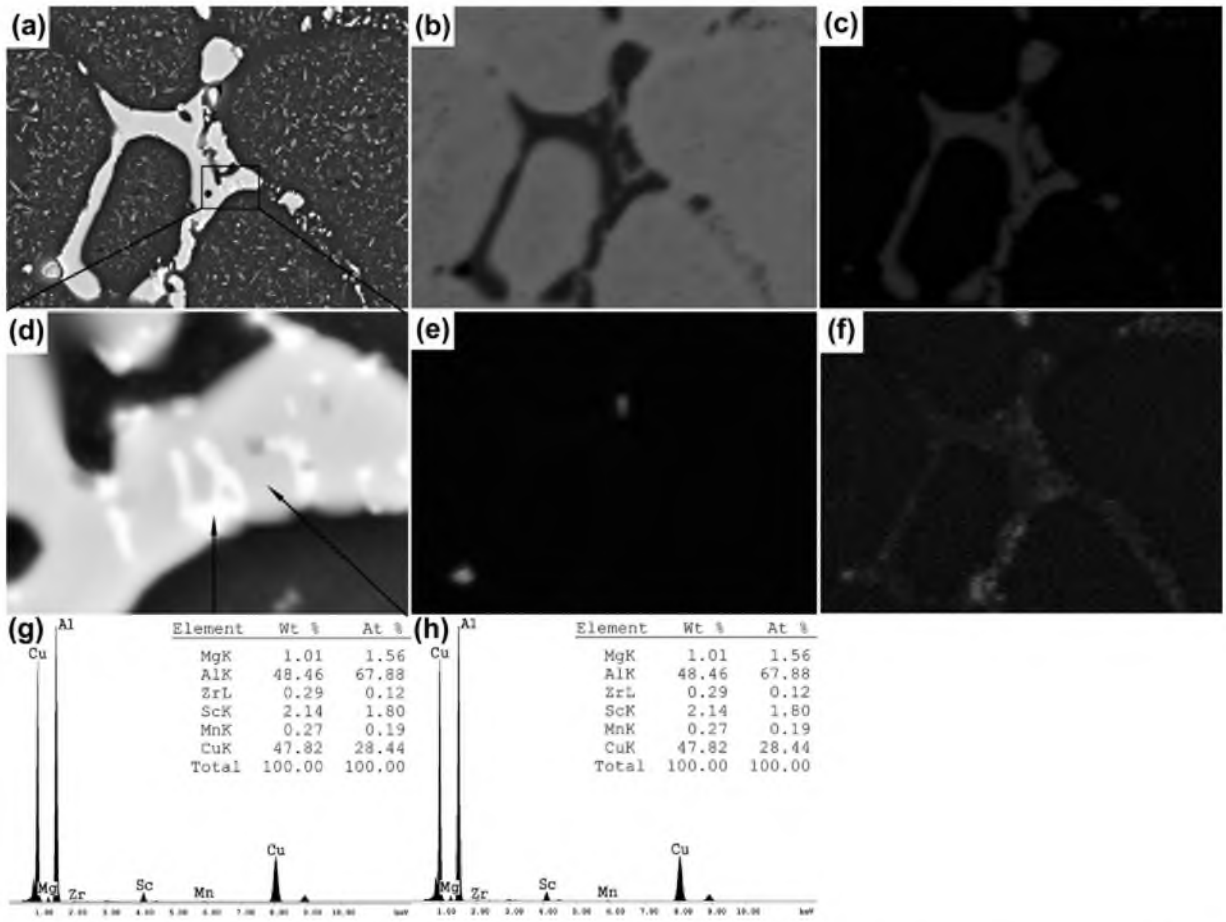

Fig. 7. SEM image of a particle after homogenised annealing (a and d); (b), (c), (e) and (f) are the distribution of element Al, Cu, Ge and Sc in the selected plane, respectively. EDX analysis of different areas of the particle (g and h).

dependent on grains that vary from 0 to 2.4%. No evidence for the coherent nano-scale dispersoids was found within numerous aluminium grains; the distribution of $Al_3(Sc,Zr)$ within the aluminium matrix is non-uniform at the meso-scale. The precipitation-free grains adjacent to precipitations of the primary θ-phase that contain Sc and the ternary W-phase were frequently observed. Fig. 6f shows that the average Sc content within the aluminium matrix is 0.09%. Therefore, about 50% of the Sc was consumed during the formation of the coarse particles after the homogenisation annealing. In contrast, almost all of the Zr remains within the supersaturated solid solution after the homogenisation annealing; a negligible part of the Zr is consumed during the formation of the W-phase.

In summary, homogenisation annealing induces dissolution of the excessive θ-phase, full dissolution of the unknown phase that contains Ag and Mg, the formation of the W-phase, and the uniform distribution of alloying elements, which includes all the silver within the aluminium matrix (Fig. 8); Ge remains in the Mg_2Ge phase.

3.2. DSC analysis

Fig. 10 shows DSC plots for the alloy in both the as-cast and homogenised states. A well-defined difference is evident in the precipitation behaviour between the two states of the Al–Cu–Mg–Ag–Sc alloy. At 532 and 565 °C, a double endothermic peak appears in the alloy after solidification, and the homogenised alloy exhibits an almost-single, distinct endothermic peak at 565 °C. At 532 °C, the endothermic peak is largely caused by the melting of the Al-θ-phase eutectic [21,29,33]. A decrease in the volume fraction of the θ-phase after homogenisation annealing leads to a significant decrease in the intensity of this peak up to a negligible value (Fig. 10b). For the alloy in the as-cast state, the DSC curve tends to be endothermic, which indicates the gradual dissolution of the θ-phase with heating. However, this process is incomplete at 532 °C, which results in partial melting. In contrast, for the alloy in the homogenised state, the DSC curve provides weak evidence for the dissolution of the θ-phase prior to the partial melting of the Al–Al_2Cu eutectic. At 532 °C, the endothermic peak in the homogenised material could also be distinguished, but the energy of the partial melting is negligible. Therefore, partial melting of the Al–Al_2Cu eutectic was almost suppressed by homogenisation annealing. Apparently, only the Al Sc-depleted θ-phase eutectic melts at 532 °C in the homogenised material. Therefore, homogenisation annealing eliminates massive melting at 532 °C.

The endothermic peak at 565 °C is attributed to the partial melting of the other high-temperature eutectic. The homogenisation annealing obviously increases the intensity of this peak. The Sc-containing θ-phase, along with the W-phase, may by responsible for this peak. Other authors have recently shown [34], using the technique for calculation of phase diagram (CALPHAD), that the invariant reaction, Liquid ↔ W-phase + Al + θ-phase, must occur at 547 °C. The difference between the melting temperature of 547 °C calculated in the previous work [34] and the endothermic peak position at 565 °C observed in the present study may be attributable to the Sc-containing θ-phase exhibiting an increased resistance to melting. No evidence for the other invariant reaction, Liquid + Al_3Sc ↔ W-phase + Al, which has been calculated to occur at ~574 °C [34], was found in the present study.

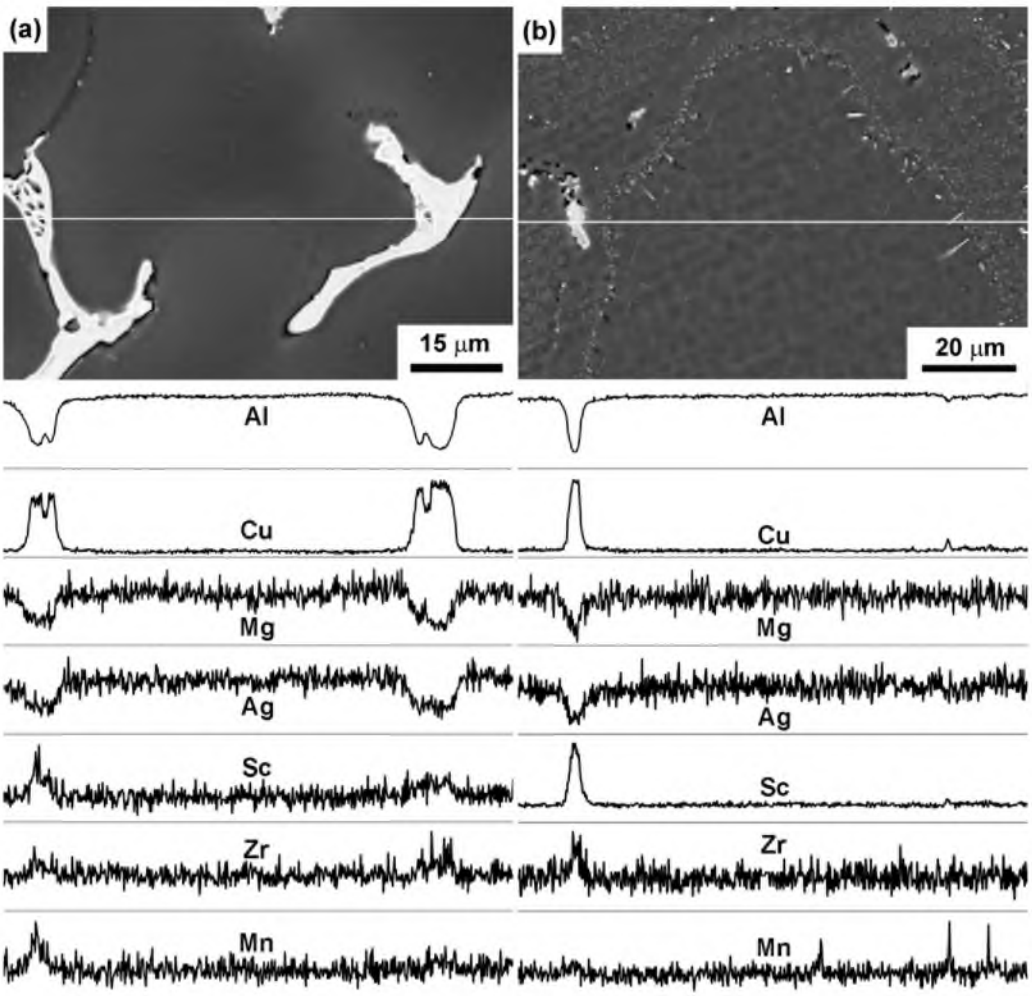

Fig. 8. SEM and composition profiles along the line indicated in the SEM image showing the number of EDX counts under the Cu, Mg, Ag, Sc, Zr and Mn peaks as a function of the position for the alloy in the as-cast state (a) and after homogenisation annealing (b).

3.3. *X-ray analysis*

The X-ray diffraction data for the alloy in the as-cast and homogenised states are shown in Figs. 11 and 12, respectively. XRD peaks that originate from the θ-phase and the Mg_2Ge phase can be distinguished in the both states of the alloy. XRD peaks that originate from the W-phase are distinguished only in the homogenised material. Therefore, the formation of the W-phase under homogenisation is supported by the XRD data.

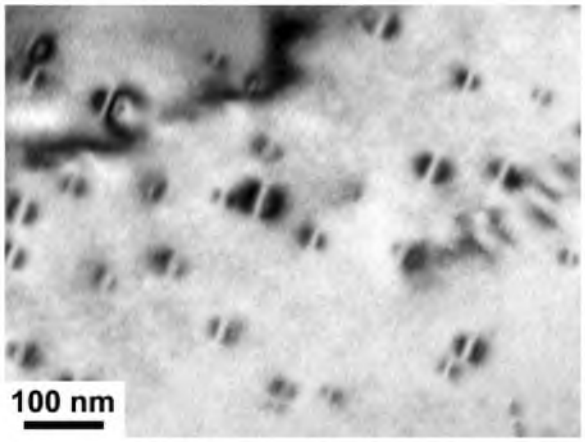

Fig. 9. $Al_3(Sc,Zr)$ particles within the aluminium matrix after homogenisation annealing.

No evidence for the Al_3Sc phase was observed either after solidification or after homogenisation annealing. It was only possible to recognise superstructure peaks that are attributable to the $L1_2$ structure of the Al_3Sc phase. Regular peaks of this phase that are associated with a fcc lattice match those that originate from the aluminium matrix, even at high values of 2θ, because the mismatch between these two crystal structures is negligible for all of the exposed crystal planes, as previously discussed [12]. However, no superstructure peaks for the Al_3Sc phase were observed. We assume that the lack of superstructure peaks results from concentration of this phase that represents less than 1% of the total mass, which is the experimental limit for the X-ray diffractometer used.

Evidence of unidentified X-ray peaks that are attributed to the other phase in the as-cast material was observed. Homogenisation annealing diminishes these X-ray peaks. We presume that these peaks, which are believed to be superstructure peaks, originate from the phase of unknown origin that contains Ag and Mg. This phase dissolves during homogenisation annealing. As previously discussed, the θ-phase and Ω-phase are, in fact, one phase. As a result, these two phases are difficult to distinguish by XRD analysis. We assume that the phase of unknown origin that contains Mg and Ag is the θ-phase that has been enriched by these elements. This primary phase precipitates under solidification and completely dissolves during homogenisation annealing.

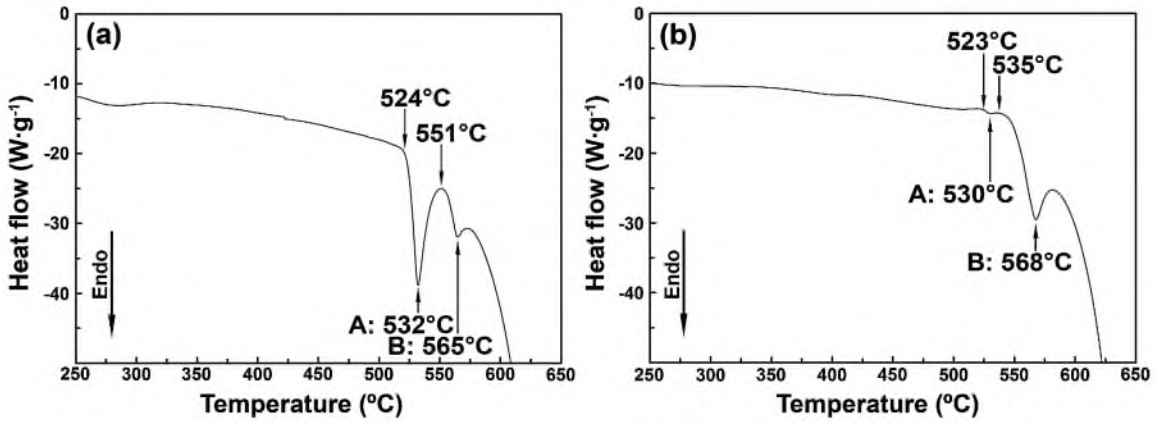

Fig. 10. DSC plots for the alloy before (a) and after (b) homogenisation annealing.

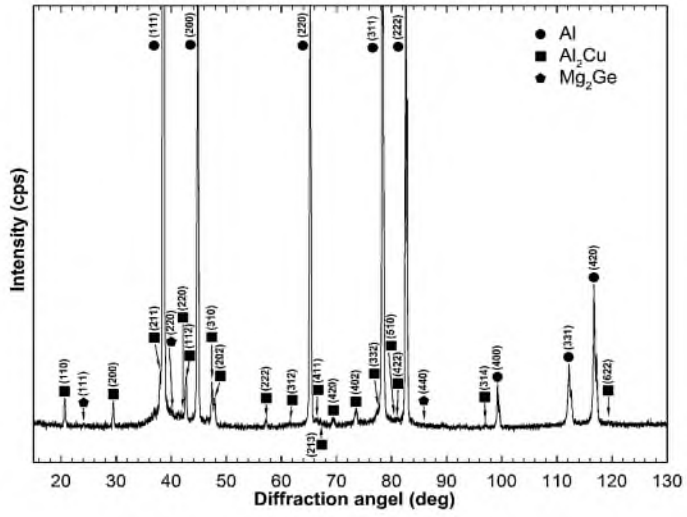

Fig. 11. X-ray diffraction traces taken from the as-cast alloy.

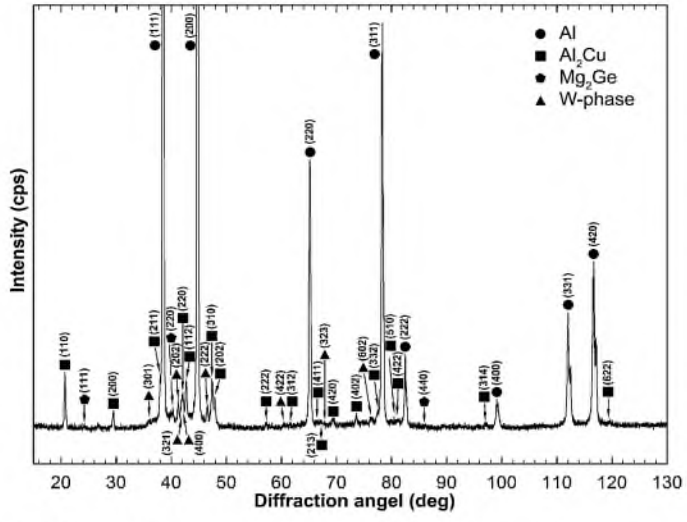

Fig. 12. X-ray diffraction traces taken from the alloy after homogenisation annealing.

4. Discussion

An inspection of the experimental data shows that the Sc additives did not lead to unusual Ag or Mg segregations; therefore, this additional alloying will not affect the size and distribution of the Ω-phase that precipitates during artificial ageing. In turn, no effects of silver on the precipitation of the Al_3Sc phase were observed. Therefore, there is no unique solidification behaviour of Sc-containing aluminium alloys in the Al–Cu–Mg–Sc system. The regularities of the solidification behaviour and decomposition of Al–Sc solid solutions under homogenisation annealing for alloys belonging to the Al–Cu–Sc [12,18,19,21] and Al–Cu–Mg–Ag–Sc systems are essentially the same.

The following regularities of the solidification behaviour and structural evolution of the present alloy are emphasised:

(i) No formation of the primary Al_3Sc phase occurs during solidification. Nanoscale, coherent particles of $Al_3(Sc,Zr)$ precipitate during homogenisation annealing.
(ii) Primary precipitations of the θ-phase are enriched by Sc, which leads to the formation of the W-phase within these particles or/and on their interfaces during homogenisation annealing. This process consumes Sc fixed within the supersaturated solid solution and/or segregated within the primary particles of the θ-phase. As a result, $Al_3(Sc,Zr)$-free zones appear around coarse W-phase particles. The existence of these zones deteriorates the alloy's strength.

The W-phase exhibits a significantly lower Gibbs energy than does the Al_3Sc phase [34]. Therefore, under any high-temperature annealing, the coarse particles of the W-phase will grow by consuming Sc that is fixed within the supersaturated solid solution or by dissolving $Al_3(Sc,Zr)$ dispersoids. No appearance of the W-phase can be tolerated in Sc-containing Al-Cu alloys that are intended for high-temperature applications.

In addition, data from the present work show that the W-phase is the more stable phase compared to the Sc-enriched θ-phase (0.6–1.5%), which is, in fact, a metastable phase. Homogenisation annealing leads to the dissolution of the Sc-enriched θ-phase; the equilibrium θ-phase contains 0.1% Sc or less.

Two methods of preventing the formation of the W-phase in Al-Cu-Sc alloys are known. First, an increase in the Sc content up to 0.5–0.8% effectively suppresses the formation of the W-phase [12,13,15]; Al_3Sc primary particles form during solidification. As previously discussed, these particles act as effective nucleation sites for α-Al and provide a dramatic grain refinement under solidification. Grain size decreases by a factor of approximately 10 because of the formation of Al_3Sc primary particles [11–15]. However, these particles, which exhibit irregular shapes, significantly diminish the crack-propagation resistance of the alloys. Alloys of the Al–Cu–Mg–Ag system are aviation-grade materials, and low crack-propagation resistance severely restricts their commercial applications. In addition, an increased Sc content significantly

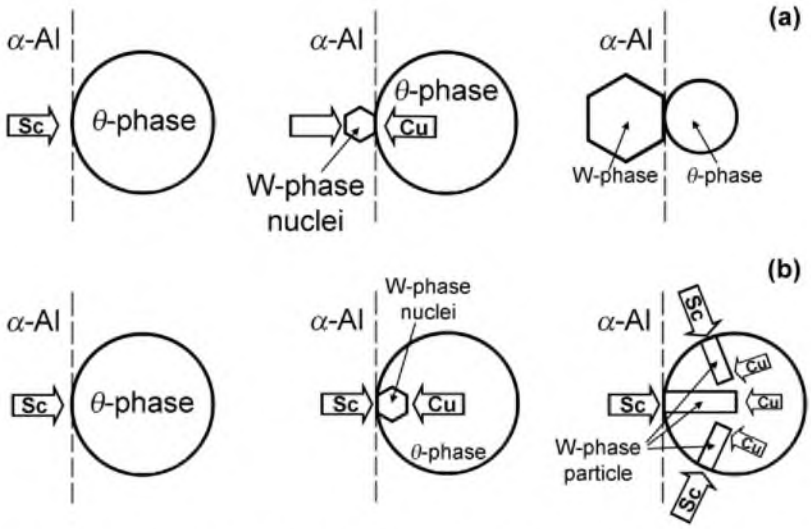

Fig. 13. Formation of the W-phase by nucleation on the θ-phase (a) and by transformation from θ-phase to the W-phase (b).

increases the material costs. Therefore, this is not a suitable method for the production of aviation-grade aluminium alloys.

Second, the formation of the Sc-enriched θ-phase during solidification, which will cease the formation of the W-phase under homogenisation annealing, can be suppressed by decreasing the copper content in the alloy. As previously shown [11,12,19,21,22], the W-phase does not nucleate directly within the Al matrix, even though it is thermodynamically more stable than Al_3Sc [34]. We assume that homogeneous nucleation in a solid solution of the W-phase is impossible, even at pre-melting temperatures. A possible explanation for this behaviour has been observed in the complex, highly ordered crystal structure of this phase [12,19,21,22], which makes the probability for the formation of a critical nucleus much lower for the W-phase than for Al_3Sc, although Al_3Sc exhibits a simpler crystal structure [13–17]. The θ-phase and W-phase exhibit tetragonal lattices (*I4/mmm*). However, the lattice of the W-phase is more complicated because of the presence of Sc [19]. Therefore, the elimination of the primary Sc-enriched θ-phase particles may suppress the formation of the W-phase because their presence within the Al matrix is a necessary condition for W-phase formation.

The SEM observations suggest that the nucleation of the W-phase is closely related to the pre-existing θ-phase (Fig. 13). The W-phase nucleation mechanism could involve either nucleation on an existing θ-phase particle (Fig. 13a) or the transformation of the θ-phase into the W-phase by Sc diffusion from the Al matrix into the θ-phase (Fig. 13b). In the case of nucleation on the θ-phase (Fig. 13a), the W-phase constituents (Sc and Cu) must be present in the Al matrix to form a nucleus at the θ-phase/Al interface. This interface represents a preferred nucleation site because the incoherent interface with the θ-phase reduces the interfacial energy (Fig. 13a). After the W-phase has nucleated, it will grow by consuming the θ-phase particle next to it by diffusion of Sc and Cu through the Al matrix. The θ-phase/W-phase interface will remain fixed until the θ-phase is completely dissolved.

In the case of the transformation mechanism, Sc diffuses into the θ-phase particle itself, which increases the Sc content by a factor of 4 or more and leads to the transformation of the crystal lattice of the θ-phase to the lattice of the W-phase. During the diffusion, a concentration gradient will appear between the areas of the θ-phase and the areas of the W-phase; Sc depletes the θ-phase and enriches the W-phase. In addition, growth of the W-phase consumes Sc that is fixed within the supersaturated solid solution and consumes Cu by dissolution of the excess Sc-enriched θ-phase. This mechanism of the formation of the W-phase is apparently dominant.

Sc and Zr additives hinder the formation of the primary θ-phase in the Al–4.5% Cu alloy [12]. A careful inspection of previously reported data [12,19,21,22,33–36] reveals that no precipitation of the primary θ-phase is expected in the Sc- and Zr-containing Al–Cu alloy at a cooling rate of 100 K/s or greater. Therefore, the optimal chemistry of Sc-containing Al–Cu alloys is Al–4–4.5Cu–0.45Mg–0.4Ag–0.17Sc–0.09Zr. Mg and Ag exhibit no relation to the formation of the W-phase; therefore, these elements can be added to this alloy in a conventional ratio of Cu/Mg = Cu/Ag = 10/1 [2–8]. It is reasonable to increase the Sc/Zr ratio to 1.8–2 to induce the formation of the coherent $Al_3(Sc,Zr)$ dispersoids, but the Sc is expended during the formation of coarse particles of the aforementioned equilibrium phases that contain Sc.

An inspection of experimental results shows that Ge additives led to the precipitation of the primary Mg_2Ge phase, which could not be dissolved by subsequent homogenisation annealing. Thus, additional alloying by Ge is not suitable for the Al–Cu–Mg–Ag–Sc alloys. It is impossible to modify Al–Cu–Mg–Ag alloys by Ge additives to refine particles of the Ω-phase in Al–Cu–Mg–Ag alloys.

5. Conclusions

The addition of Sc and Ge to Al–Cu–Mg–Ag alloys leads to extremely diverse solidification behaviours of this alloy.

(1) Under solidification, the precipitation of the primary θ-phase enriched with Sc occurs. No precipitations of the ternary W-phase ($Al_{8-x}Cu_{4+x}Sc$) was found. Approximately 70% of the Sc and all of the Zr were fixed within the supersaturated solid solution.
(2) Under homogenisation annealing, the formation of the W-phase as coarse particles occurs. The formation of the W-phase leads to the dissolution of the Sc-enriched θ-phase and to the depletion of Sc from the supersaturated solid solution. The precipitation of nano-scale $Al_3(Sc,Zr)$ coherent dispersoids precipitated within the Al matrix, which occurs inhomogeneously because of the formation of precipitation-free zones around coarse W-phase particles, consumes 50% of the overall Sc.
(3) Ge precipitates as the Mg_2Ge-phase under solidification. This phase could not be dissolved by homogenisation annealing.

Acknowledgements

This study was supported by the Federal Agency for Education, Russia, under grant No. P875. The authors are grateful to the staff of the Joint Research Center, Belgorod State University, for their assistance with the mechanical and structural characterisations.

References

[1] I.J. Polmear, G. Pons, Y. Barbaux, H. Octor, C. Sanchez, A.J. Morton, W.E. Borbidge, Rogers, Mater. Sci. Technol. 15 (1999) 861–868.
[2] S.P. Ringer, K. Hono, I.J. Polmear, T. Sakurai, Acta Mater. 44 (1996) 1883–1898.
[3] L. Bakavos, P.B. Prangnell, B. Besb, F. Eberl, Mater. Sci. Eng. A491 (2008) 214–223.
[4] B.C. Muddle, I.J. Polmear, Acta Metall. 37 (1989) 777–789.
[5] R.W. Fonda, W.A. Cassada, G.J. Shiflet, Acta Met. Mater. 40 (1992) 2539–2546.
[6] L. Reich, M. Murayama, K. Hono, Acta Mater. 46 (1998) 6053–6062.
[7] Y.C. Chang, J.M. Howe, Met. Trans. 24 (1993) 1461–1470.
[8] R.N. Lumley, A.J. Morton, I.J. Polmear, Acta Mater. 50 (2002) 3597–3608.
[9] M. Vural, J. Caro, Mater. Sci. Eng. A520 (2009) 56–65.
[10] J. Wang, X. Wu, K. Xia, Mater. Sci. Eng. A 234–236 (1997) 287–290.
[11] Y. Li, Z. Liu, Q. Xia, Y. Liu, Metall. Mater. Trans. 38 (2007) 2853–2858.
[12] A.F. Norman, P.B. Prangnell, R.S. McEwen, Acta Mater. 46 (1998) 5715–5732.
[13] K.B. Hyde, A.F. Norman, P.B. Prangnell, Acta Mater. 49 (2001) 1327–1337.
[14] J. Røyset, N. Ryum, Intern. Mater. Rev. 50 (2005) 19–44.
[15] D.H. Xiao, M. Song, B.Y. Huang, J.H. Yi, Y.H. He, Y.M. Li, Mater. Sci. Technol. 25 (2009) 747–752.
[16] D.N. Seidman, E.A. Marquis, D.C. Dunand, Acta Mater. 50 (2002) 4021–4035.
[17] M.E.V. Dalen, D.N. Seidman, D.C. Dunand, Acta Mater. 56 (2008) 4369–4377.
[18] E.A. Marquis, D.N. Seidman, Acta Mater. 53 (2005) 4259–4268.
[19] L.S. Toropova, D.G. Eskin, M.L. Kharakterova, T.V. Dobatkina, Advanced Aluminum Alloys Containing Scandium: Structure and Properties , Taylor & Francis, 1997.
[20] K.L. Kendig, D.B. Miracle, Acta Mater. 50 (2002) 4165–4175.
[21] M.L. Kharakterova, Russ. Metall. 4 (1991) 195–199.
[22] M.L. Kharakterova, D.G. Eskin, L.S. Toropova, Acta Metall.Mater. 42 (1994) 2285–2290.
[23] W. Lefebvre, F. Danoix, H. Hallem, B. Forbord, A. Bostel, K. Marthinsen, J. Alloys Compd. 470 (2009) 107–110.
[24] M. Vlach, I. Stulíková, B. Smola, N. Zaludová, J. Cerná, J. Alloys Compd. 492 (2010) 143–148.
[25] A. Deschamps, L. Lae, P. Guyot, Acta Mater. 55 (2007) 2775–2783.
[26] S.P. Ringer, K.S. Prasad, G.C. Quan, Acta Mater. 56 (2008) 1933–1941.
[27] M.R. Gazizov, V.V. Zakharov, R.O. Kaibyshev, V.V. Teleshov, Tech. Light All. 4 (2010) 27–35.
[28] I. Mazurina, T. Sakai, H. Miura, O. Sitdikov, R. Kaibyshev, Mater. Sci. Eng. A473 (2008) 297–305.
[29] X.Y. Liu, Q.L. Pan, X. Fan, Y.B. He, W.B. Li, W.J. Liang, J. Alloys Compd. 484 (2009) 790–794.
[30] G.A. Chadwick, Metallography of Phase Transformations , Butterworth, London, 1972.
[31] L. Cipolla, H.K. Danielsen, D. Venditti, P.E. Nunzio, J. Hald, M.A.J. Somers, Acta Mater. 58 (2010) 669–679.
[32] R. Kaibyshev, K. Shipilova, F. Musin, Y. Motohashi, Mater. Sci. Eng. A396 (2005) 341–351.
[33] F. Ma, Z. Liu, Int. J. Mod. Phys. B 23 (2009) 855–862.
[34] H. Bo, L.B. Liu, Z.P. Jin, J. Alloys Compd. 490 (2010) 318–325.
[35] N. Saunders, in: I. Ansara, A.T. Dinsdale, M.H. Rand (Eds.), COST-507: Thermochemical Database For light Metal Alloys, European Communities, Luxemburg, 1998, pp. 28–33.
[36] V.T. Witusiewicz, U. Hecht, S.G. Fries, S. Rex, J. Alloys Compd. 385 (2004) 133–143.